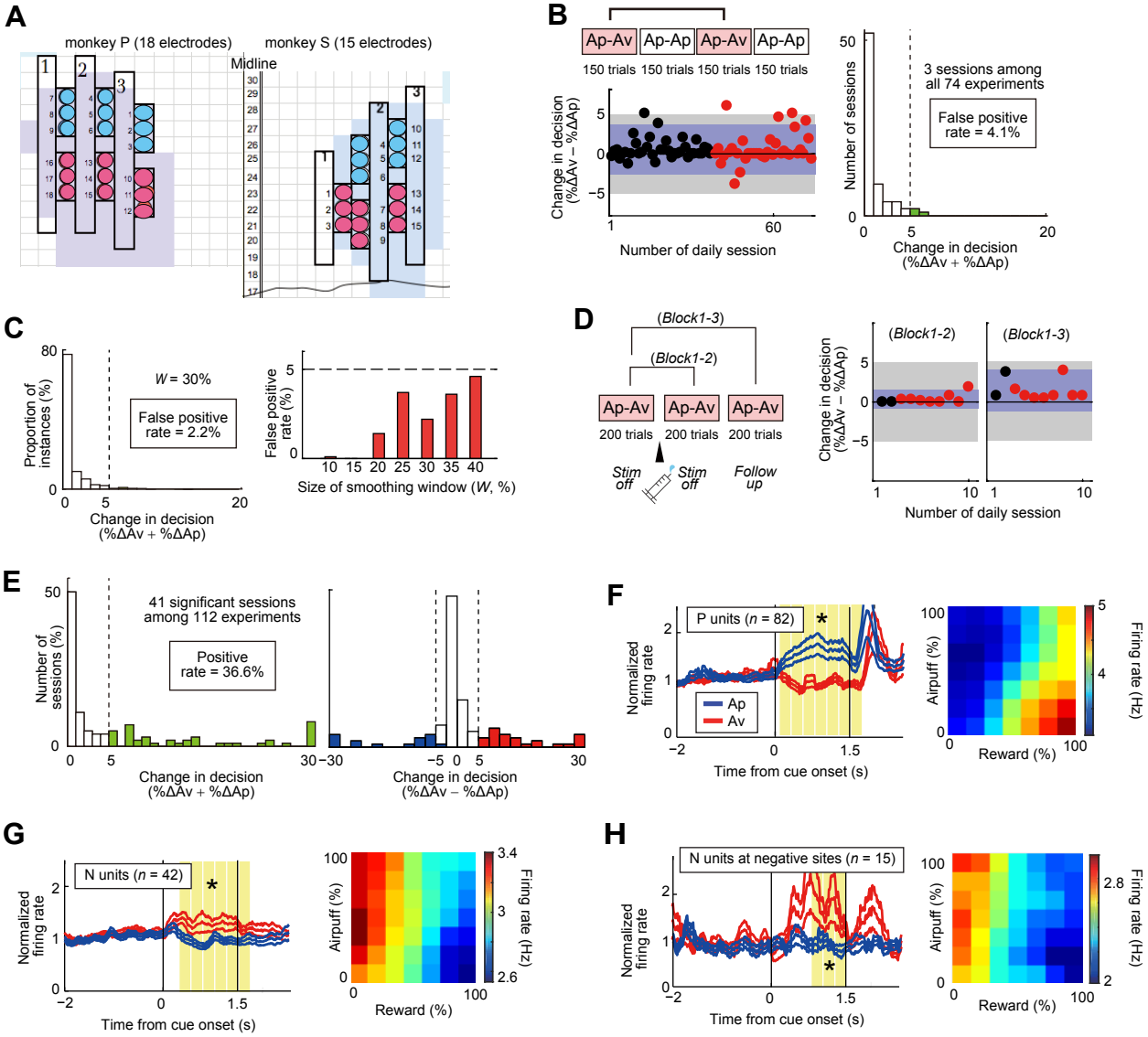

Figure S1. CN Microstimulation Induced Persistent Pessimistic State, Related to Figure 1.
(A) The positions of the implanted electrodes (circles) on the recording grid system for monkey P (left) and monkey S (right). Colored circles (cyan and magenta) indicate the two groups of electrodes used for the local average reference. Grids were placed on the skull with 5° tilt from the horizontal plane. Electrodes were implanted in the anterior portion of the CN (light blue shading). The numbers along the midline indicate the intra-aural anterior-posterior coordinates of the grid system in millimeter.
(B) Stability of Ap-Av choices in recording-only sessions. Task blocks in the recording sessions (top left). We compared the choice behaviors in two Ap-Av blocks separated by 150 Ap-Ap trials. Change in decision frequencies was quantified by (%ΔAv − %ΔAp) (bottom left). Black and red circles indicate the sessions with monkeys S and P, respectively. Purple region denotes the 95% confidence interval. Gray shading indicates the 5% discrimination threshold. The distribution of the change in decision frequencies quantified by (%ΔAv + %ΔAp) (right). If we set the significance level to be 5% of the decision matrix, the false positive rate became 4.1%.
(C) False positive rates for different window sizes. The distribution of (%ΔAv + %ΔAp) in the samples produced by the logit model (W = 30%) (left). False positive rate was 2.2 % with the 5% threshold (right).

(D) Stability of Ap-Av choices in no-stimulation sessions, illustrated with task block design (left) and choice behaviors in the 200 trials after the saline injection compared with those in the 200 trials before the injection (right).
(E) Definition of effective sessions. The distribution of total change (i.e., %ΔAv + %ΔAp) in the 112 stimulation sessions (left). Forty-one sessions exceeded the 5% criterion (green). The distribution of (%ΔAv − %ΔAp) in the 112 stimulation sessions (right). Blue and red color indicated the sessions that were classified as significant by the criterion in the left panel (red: increase in Av, blue: increase in Ap). Only one session, in which the total fraction was larger than –5% in the right panel, was classified as effective.
(F) Mean (± SEM) spike density of P units (n = 82) (left). For each unit, spike density activities for upcoming Ap (red) and Av (blue) choices was normalized by the firing rate during the precue period before being averaged. For each 250-ms bin, we tested whether the mean firing rate for Ap choice was different from that for Av choice. The bin in which the mean activity showed significant difference (*$p < 0.05$, t-test) was highlighted by light yellow. Mean activity in the decision matrix (right). The cue-period activity of each unit was binned to an 8-by-8 matrix before being averaged.
(G) Mean (± SEM) spike density of N units (n = 42).
(H) Mean (± SEM) spike density of N-type units recorded within a 1-mm bin at the negative effective sites. These units showed differential activities for Ap and Av choices during the late phase of the cue period. *$p < 0.05$ (two-tailed t-test).

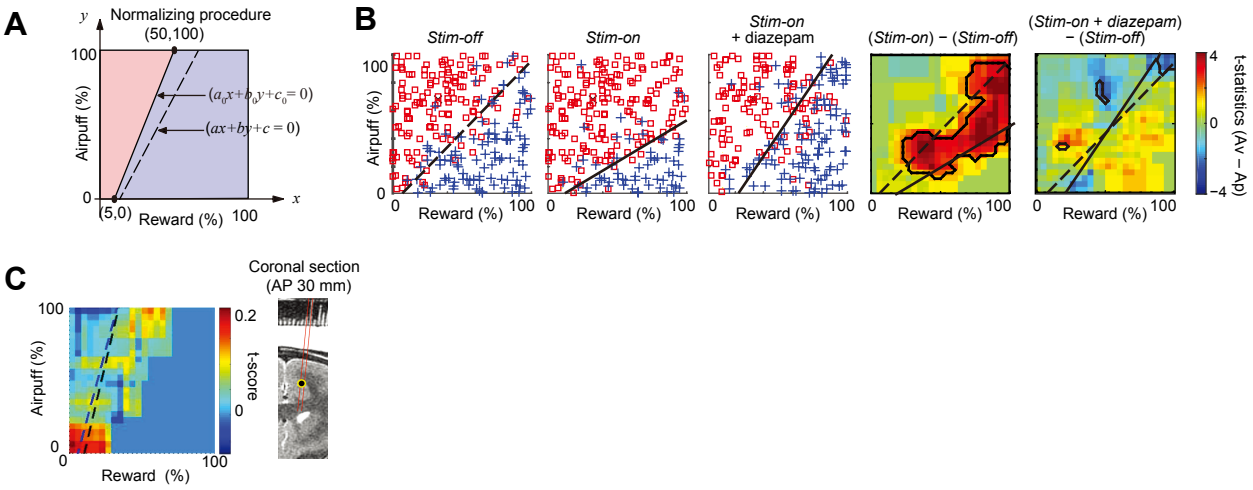

Figure S2. Microstimulation of Negative Effective Sites Induced Persistent Negative States, Related to Figure 2.

(A) Normalization procedure to calculate the standardized decision boundary (see STAR Methods).

(B) Example of diazepam administration that blocked stimulation-induced increase in Av choices. Panels show, from left to right, decision matrix for the first 200-trial block without stimulation (*Stim-off*), the second trial block during which stimulations (150 μA) were applied (*Stim-on*), and the third trial block after diazepam administration (0.25 mg/kg, IM) (*Stim-on* + diazepam). Stimulation effect was measured by difference in the decision matrix (i.e., (*Stim-on*) – (*Stim-off*)), and the blockade was measured by ((*Stim-on* + diazepam) – (*Stim-off*)).

(C) Microstimulation around rCMA (black dot in the right panel) elicited arm movement but did not change decision. Left panel shows the t-statistic representing difference between decision matrices in the *Stim-off* and *Stim-on* blocks. Note that the maximum t-statistic (i.e., the difference in decision) is less than 0.2, showing no significant change in decision frequencies.

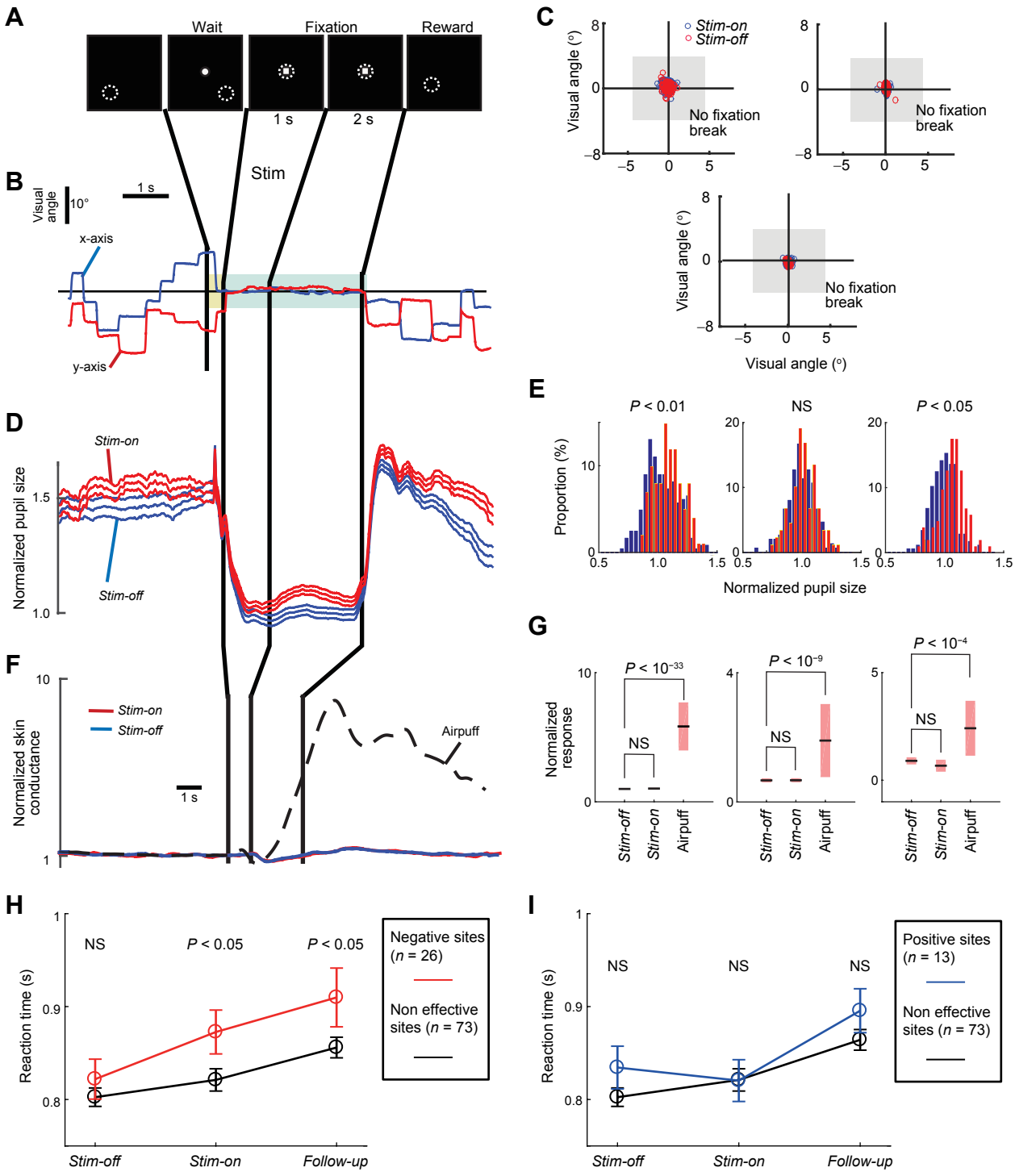

Figure S3. Microstimulation of Effective CN Sites Did Not Induce Eye Movements, but Caused Detectable Pupillary Dilation in One of Three Experiments (Control Experiment 3), Related to Figure 2.

(A) Fixation task. See STAR Methods for details.

(B) Eye position (blue: x-axis, red: y-axis) around the central fixation point (black horizontal line) in a representative single trial.

(C) The mean eye position during the 3-s fixation period in the *Stim-on* (red) and *Stim-off* (blue) trials. Each panel represents the data from one session performed with stimulation at one of three different negative effective sites. A gray square denotes the fixation window (5° x 5°). Stimulation induced no fixation break.
(D) The mean (± SEM) pupil size for the *Stim-off* (red) and *Stim-on* (blue) trials in one session.
(E) The distribution of mean pupil size during the 3-s fixation period in three individual sessions. Outside the fixation period, the pupil size estimated by video monitoring (Eyelink 1000; SR Research) was not necessarily accurate due to eye movements, variation in depth of focus, or change in brightness. We thus compared the pupil sizes recorded during the fixation period. Mean of the distribution for the *Stim-on* (yellow bars) and *Stim-off* (blue bars) trials were compared by two-sampled t-tests. In two experiments, the pupils were significantly dilated by the stimulation ($p < 0.05$), suggesting a physiological response induced by the stimulation.
(F) Skin conductance averaged over the *Stim-on* (red) and *Stim-off* (blue) trials, compared with that responding to an unexpected airpuff delivered out of the task (dashed line).
(G) Significant changes in the skin conductance was induced by unexpected airpuff, but not by the stimulation ($p < 10^{-4}$, t-test), suggesting that the stimulation itself did not produce any physiological responses related to aversive perception comparable to those induced by airpuff. Horizontal black lines indicate the mean, and pink shading indicates SEM. Each of three panels indicates the result of each session.
(H) Mean RTs averaged over each block were not significantly different between negative effective (red) and non-effective (black) sites in the *Stim-off* block, but they were significantly different in the *Follow-up* and *Stim-on* blocks ($p < 0.05$, t-test).
(I) Positively effective microstimulation induced no detectable change in RT. Mean RTs were not different between positive effective (blue) and non-effective (black) sessions for each block.

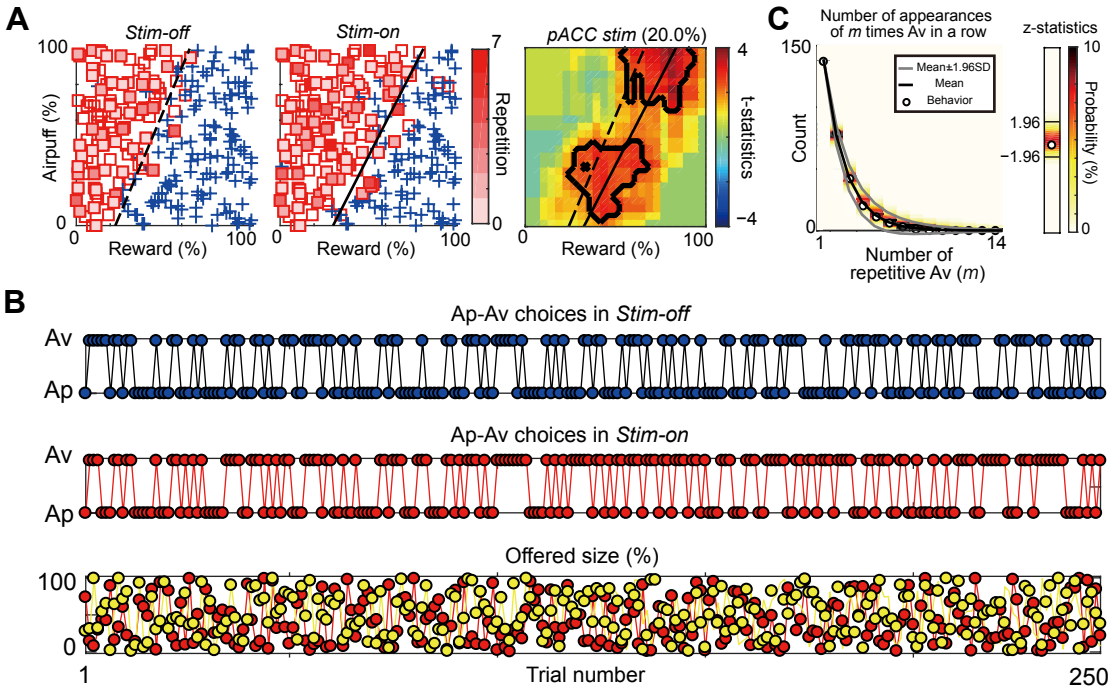

Figure S4. Computational Models Could Predict the Repetitive Choices in pACC Stimulation, Related to Figure 4.

(A) Ap (blue cross) and Av (red square) choices in the *Stim-off* (left) and *Stim-on* (middle) blocks in the same session. Stimulation of pACC increased Av choices by 20.0% (right).

(B) Sequences of the Ap-Av decisions in the *Stim-off* (top) and in the *Stim-on* (middle) blocks, and the sequence of the reward (red circles) and airpuff (yellow circles) sizes (bottom).

(C) Comparison between the observed number of repetition in the *Stim-on* block and the expected number of repetition derived from the RR procedure, illustrated as in Figure 3C.

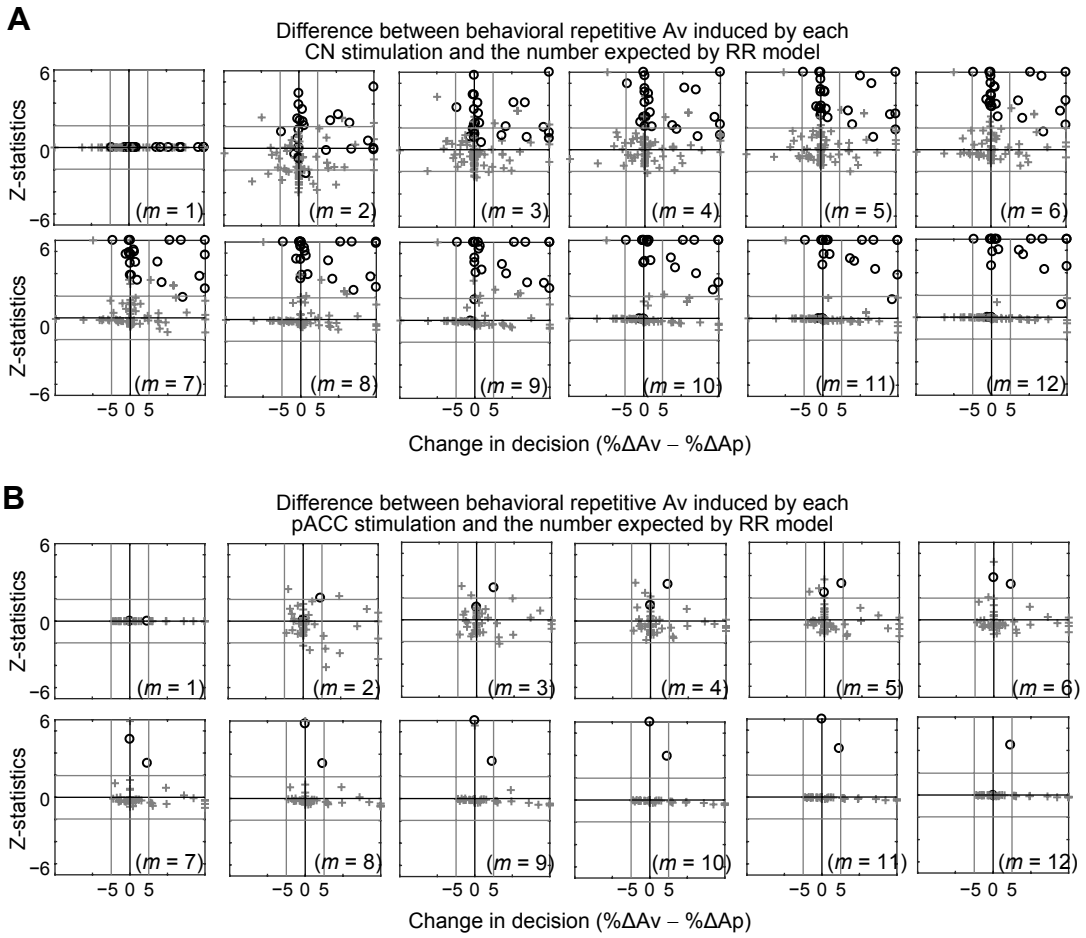

Figure S5. Difference between Repetitive Av Behaviors and Prediction of RR Procedure, Related to Figure 4.

(A) Comparisons between the observed number of repetition induced by each CN stimulation and the number expected by the RR procedure, as a function of change in decision frequencies (%ΔAv − %ΔAp). For each session, we calculated the z-statistics representing the deviation from the model for each session for each repetition number (*m*). Circles indicate the sessions in which the stimulation induced significant deviation from the model ($p < 0.05$, z-test), and gray crosses represent non-significant sessions. Data points at the ceiling indicate that they are over the ceiling.

(B) Comparison between the observed number of repetition induced by each pACC stimulation and prediction of the RR model.

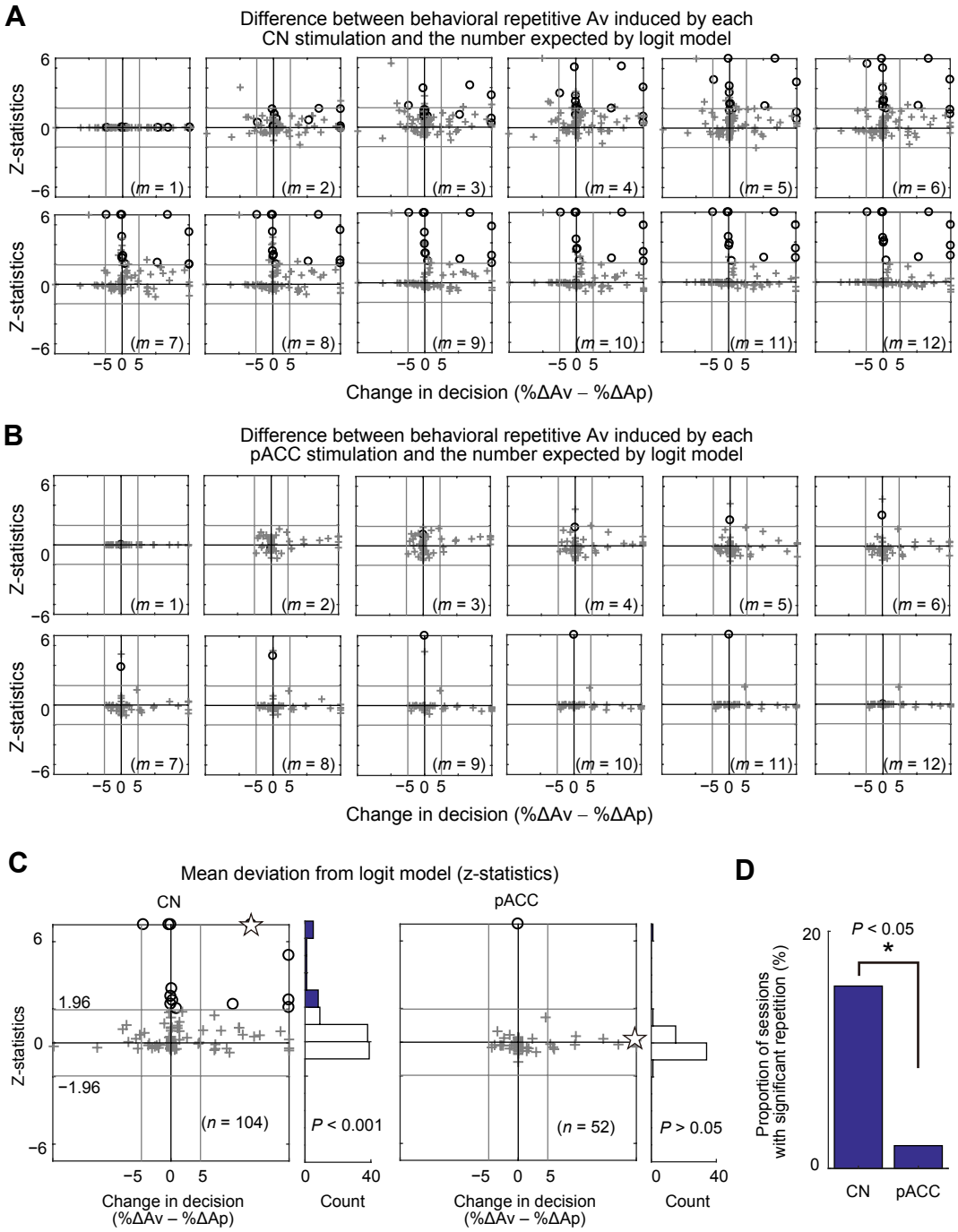

Figure S6. Logit Model Produced the Same Results as RR prediction, Related to Figure 4.
(A) Comparison between the observed number of repetition induced by each CN stimulation and the expected number of the logit model. Using the model, we produced the choice sequence based on a sequence of 10,000 offers without any influence of the previous choice sequence, derived the distribution of repetitive *m*-time Av choices.
(B) Comparison between the observed number of repetition induced by each pACC stimulation and prediction of the logit model.
(C) Mean deviations in repetitive Av choices, measured in z-statistics, from the logit model during sessions with CN (left) or pACC (right) stimulation, plotted against changes in decision (%ΔAv − %ΔAp).

Circles indicate the sessions in which the stimulation induced significant deviation from the model ($p < 0.05$, z-test), and gray crosses are non-significant sessions. Stars indicate the sessions shown in Figures 3 and S4. Data points beyond the y-axis range are shown at the ceiling. Bars at right show the distribution of the mean deviations.
(D) Proportion of sessions that showed significant deviations from the logit models ($p < 0.05$, z-test). Proportion in the CN stimulation experiments was significantly larger than that in the pACC experiments (Fisher's exact test).

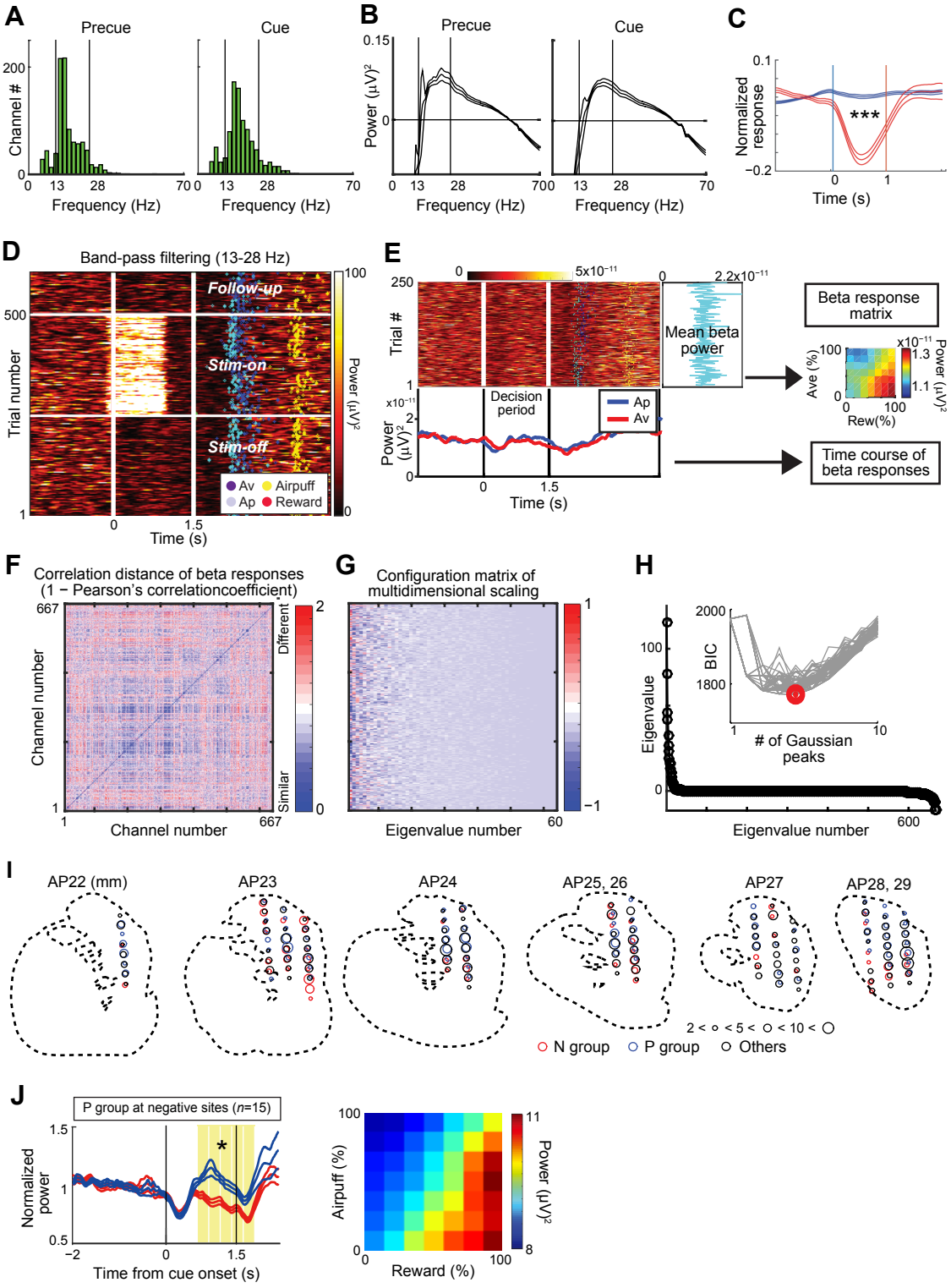

Figure S7. Procedure to Analyze Beta Oscillations in Recorded LFPs, Related to Figures 5 and 6.
(A) Distribution of peak frequencies for all LFPs recorded during *Stim-off* blocks. For the LFPs in the precue (left) or cue (right) periods, the peak frequency of the maximum spectral power density in the baseline-subtracted LFP was derived. The peak frequencies of many LFPs were distributed within the beta range (13-28 Hz).

(B) Mean (± SEM) power spectrum of all *Stim-off* LFPs (n = 958) for the precue (left) and cue (right) periods after subtracting the fitted pink noise spectrum.
(C) Saccadic eye movement did not induce beta suppression. We examined the change in beta magnitude triggered by each saccadic eye movement (i.e., saccade-triggered beta responses), and compared between saccade-triggered (blue) and cue-triggered (red) beta responses in 183 channels. Lines represent the average (± SEM) beta magnitude normalized relative to the 1-s period before the saccade or cue onset. Distribution of the normalized magnitudes for saccade-triggered responses (averaged in 1-s period after the saccade) and those for cue-triggered responses were significantly different. ***$p < 0.001$ (two-sample Kolmogorov-Smirnov test).
(D) Band-pass filtering was performed for the LFPs of the same channel as in Figure 5A, and the band-pass filtered power is plotted according to color scale at right. The high power values recorded during the first 1 s of the cue period in the Stim-on block are due to electrical stimulation artifact. To portray the beta-band power in the decision matrix, beta-band power was averaged over the cue period for each trial. In the response and outcome periods, the time of Ap (purple), Av (cyan), airpuff delivery (yellow) and reward delivery (red) was variable because their occurrence was dependent on the monkey's response.
(E) Analysis procedure to derive beta response matrices. From the band-pass (13-28 Hz) filtered LFPs, mean beta power during the cue period was calculated for each trial, and were mapped to the 8-by-8 decision matrix to produce a beta response matrix, which were subsequently used for classification of the beta responses shown in Figure 5C. The time courses of power of beta responses were averaged separately for Ap and Av choices, and were later used to calculate the time course of beta power as shown in the bottom panel of Figure 6A.
(F) Matrix of correlation distance between pairs of all beta response matrices ($D = [d_{ij}]$). The color of each element shows the correlation distance ($d_{ij} = 1 - r_{ij}$), where rij is the cross-correlation between decision matrices of beta response *i* and response *j*.
(G) Configuration matrix returned by multidimensional scaling function (*cmdscale* function of MATLAB).
(H) The eigenvalue representing the explanatory power of each feature dimension. Inset shows the BIC values for different numbers of Gaussian peaks. BIC values for each fitting are shown as gray lines. The minimum BIC was given by five Gaussian peaks and denoted as red circle.
(I) Spatial distribution of sites at which we recorded LFPs classified as N (red), P (blue), and other (black) groups. The size of each circle indicates the number of LFPs at the location. Data from monkey S were projected onto outline drawings of striatum of monkey P.
(J) Mean power magnitude of P-group beta responses recorded within a 1-mm bin at the negative effective sites. Left panel shows the time course of the mean response. The mean beta response exhibited significantly differential magnitudes for Ap and Av choices in the late phase of the cue period (*$p < 0.05$, two-tailed t-test). Right panel shows the mean magnitude in the decision matrix. The cue-period activity of each beta response was binned to an 8-by-8 matrix before being averaged. Each panel was illustrated as in Figure S1F.

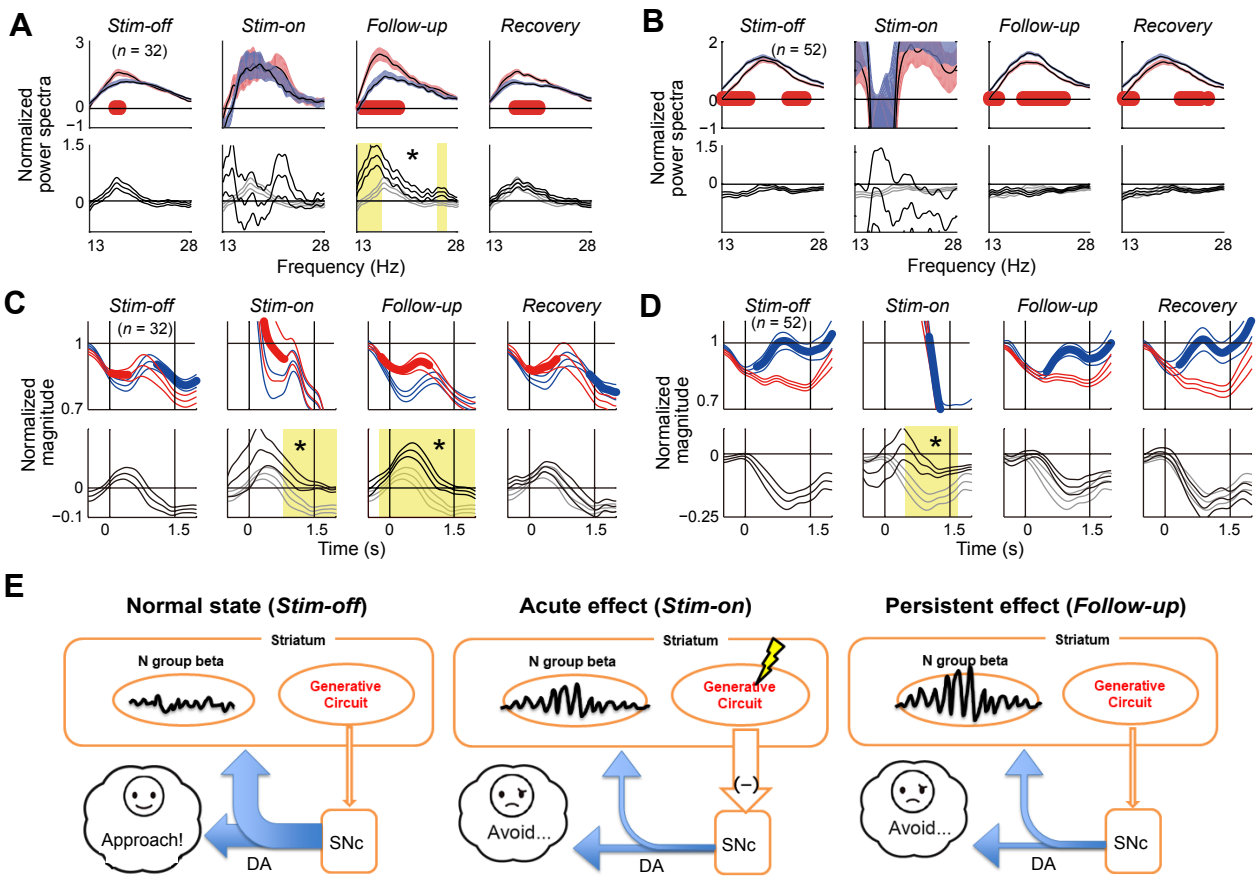

Figure S8. Modulation of Power Spectra in Effective Sessions, Related to Figure 7.
(A) Power spectra of 32 N-f channels, which were classified as N group in the *Follow-up* block. Top: Mean (± SEM) power spectra for upcoming Ap (blue) and Av (pink) choices. Power spectra were subtracted by the fitted pink noise baseline and normalized by the mean of Ap spectra in each block. Red highlights on x-axis indicate significantly larger Av power than Ap power ($p < 0.05$, two-tailed t-test, Bonferroni corrected). Bottom: Mean (± SEM) Av-Ap tuning indices derived by subtracting the Ap spectra from the Av spectra for each block (black). The Av-Ap tuning indices in the *Stim-off* block were also drawn for comparison (light gray). Yellow shading indicates the frequency range in which the Av-Ap tuning index was significantly greater than that in the *Stim-off* block, indicating that the enhancement of selectivity for Av choice in low-beta range (13-15 Hz) in N-f channels. *$p < 0.05$ (two-tailed t-test, Bonferroni corrected)
(B) Power spectra of 52 channels that did not belong to N group in the *Follow-up* block.
(C) Time-course of low-beta power magnitude for 32 N-f channels. Top: Mean (± SEM, normalized relative to precue activity) power magnitude of low-beta responses that discriminated upcoming Av (red) and Ap (blue) choices. The low-beta responses were derived by 13-18 Hz band-pass filtering of the LFPs. Thick lines on the mean values indicate times when the mean was significantly larger for Av (thick red) or Ap (thick blue) choice ($p < 0.05$, two-tailed t-test). Bottom: Mean (± SEM) Av-Ap tuning indices derived by subtracting the power magnitudes for Ap choice from those for Av power (black). The Av-Ap tuning indices in the *Stim-off* block are also drawn for comparison (light gray). Yellow shadings indicate the periods in which the tuning index was significantly greater than that in the *Stim-off* block, indicating an enhancement of selectivity for Av choice. The indices in the *Stim-on* block could be contaminated by stimulation artifacts, but the indices in the *Follow-up* block should have reflected the tendency of persistent change in beta representation. The tuning indices in the *Follow-up* block were significantly enhanced from the early phase of the cue period. *$p < 0.05$ (two-tailed t-test).

(D) Time-course of low-beta power magnitudes of 52 channels that did not belong to the N group measured in the *Follow-up* block. The low-beta responses were derived by 13-18 Hz band-pass filtering of the LFPs.
(E) Hypothetical schema showing the possible effect of stimulation of the generative circuit. As one of several possible schemes, we hypothesize that the stimulation of the generative circuit suppresses the DA or other aminergic system. Suppression of the DA system could induce an acute effect on behavioral choice patterns with gradual changes in the subjective CBR (left and middle panels). The induced DA suppression could produce a long-term change in cellular reactivity accompanied by a change in beta oscillation, specifically at the projection sites of the DA circuity in the CN (right panel). As the input and output of the DA circuitry are likely not identical, it is reasonable to observe, as we did, beta-band modulation outside of the generative circuit locus.

Table S1

Numbers of LFP Channels Recorded during the Stimulation and Recording Experiments, Related to Figure 5

<table>
<tr><td colspan="7">Total Stim-off LFPs [1]</td></tr>
<tr><td colspan="7">958</td></tr>
<tr><td>With no beta peak</td><td colspan="6">With beta-band activity during either precue or cue period</td></tr>
<tr><td>178</td><td colspan="6">780</td></tr>
<tr><td rowspan="6"></td><td>Non-task-related</td><td colspan="5">Task-related</td></tr>
<tr><td>113</td><td colspan="5">667</td></tr>
<tr><td rowspan="5"></td><td>Recorded in 74 recording-only sessions</td><td colspan="4">Recorded in 112 stimulation experiments</td></tr>
<tr><td>366</td><td colspan="4">301</td></tr>
<tr><td>Positive effective sessions</td><td colspan="2">Negative effective sessions</td><td colspan="2">Non-effective sessions</td></tr>
<tr><td>65</td><td colspan="2">102</td><td colspan="2">134</td></tr>
<tr><td></td><td>Recorded from Stim-off to Recovery blocks [2]</td><td></td><td>Recorded from Stim-off to Follow-up blocks</td></tr>
<tr><td></td><td>84</td><td></td><td>90</td></tr>
</table>

(1) For each session, we recorded from 18 implanted channels in monkey S and from 15 implanted channels in monkey P (Figure S1A). Altogether, 958 LFP activities were recorded from these implanted electrodes during 112 stimulation sessions and during 74 recording-only sessions. For the stimulation sessions, one lead of the stimulator was connected to the ground, and cathode-leading biphasic pulses were applied to the microelectrode. In the recording-only experiments, recordings were made while the monkeys performed each of the two (Ap-Av and Ap-Ap) different tasks in alternating blocks of 150 trials.

(2) Among the channels from which we recorded 102 *Stim-off* LFPs in the negative effective sessions, we could continuously record LFPs during all of *Stim-off*, *Stim-on*, *Follow-up* and *Recovery* blocks from 84 channels. From remaining 18 channels, we could not record proper LFPs during some blocks.